2015

Compendium of Thermoviscoplasticity Modeling Parameters for Materials Under Non-isothermal Fatigue

Nathan O'Nora
University of Central Florida

COMPENDIUM OF THERMOVISCOPLASTICITY MODELING PARAMETERS FOR MATERIALS UNDER NON-ISOTHERMAL FATIGUE

by

NATHAN R. O'NORA

A thesis submitted in partial fulfillment of the requirements
for the Honors in the Major Program in Mechanical Engineering
in the College of Engineering and Computer Science
and in The Burnett Honors College
at the University of Central Florida
Orlando, Florida

Spring Term 2015

Thesis Chair: Dr. Ali P. Gordon

ABSTRACT

Viscoplasticity models allow for the prediction of the inelastic behavior of materials, taking into account the rate-dependence. In order to model the response under non-isothermal conditions experienced by many components, such as those in turbomachinery, however, it is necessary to incorporate temperature-dependence. Additionally, for materials subjected to thermal shock, temperature rate-dependence is also important. The purpose of this research is to develop a method of determining Chaboche viscoplasticity parameters that allows for consistent behavior with changing temperature. A quartet of candidate materials, 304 stainless steel, IN617, DS GTD-111, and Ti6242S, were chosen for their applications in turbomachinery, such as gas turbines, nuclear, and aerospace applications. The focus of this research is geared towards establishing the temperature-dependence of the constants used in the model in order to obtain more accurate modeling of non-isothermal fatigue loadings than those achieved through linear interpolation of constants at several temperatures. The goal is to be able to more accurately predict the deformation behavior of components subjected to cyclic temperature and mechanical loadings which will ultimately allow for more accurate life prediction. The effects of orientation in directionally solidified (DS) materials is also examined in order to gain insight as to the expected behavior of parameters with changing orientation.

ACKNOWLEDGEMENTS

I would like to sincerely thank Dr. Gordon for introducing me to research through the Mechanics of Materials Research Group. His continued help and support have helped shape and advance my academic and professional careers. I would also like to thank Scott Keller and Dave Day from PSM for their advice and assistance. Finally I would like to thank various current and former MOMRG members for their help and assistance in learning various skills needed to complete this research.

TABLE OF CONTENTS

LIST OF FIGURES

LIST OF TABLES

CHAPTER 1: INTRODUCTION

Many high value components of engineering systems, such as those used in reactors and turbines, are subjected to cyclic mechanical loading. There are generally two types of components: stationary and rotary. In either case, variable mechanical loading is accompanied via thermal gradients, cyclic pressure, centrifugal loading, and/or varying temperatures [1, 2]. In order to withstand the harsh conditions of these environments, numerous high strength materials are used including steels, Ni-based superalloys, and titanium alloys [3]. Obtaining accurate life predictions for these components is important for reducing maintenance costs of these parts without increasing the risk of failure. Constitutive models are often employed to acquire the parameters essential for modeling such as stress range, $\Delta\sigma$, mean stress, σ_m, inelastic strain range, $\Delta\varepsilon_{in}$, and hysteresis energy, ΔW. An example of a typical hysteresis loop where a viscoplasticity model may be explored is shown in Figure 1. Improvements in the abilities of constitutive models to simulate material behavior under the non-isothermal loading experienced by many components will confer more accurate life predictions.

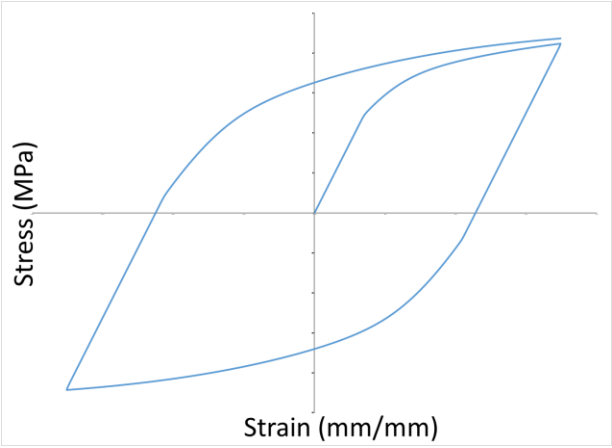

Figure 1: Example of a typical hysteresis loop used in exploring viscoplasticity models

In order to examine the temperature-dependence of the cyclic behavior exhibited by materials, data for cyclic mechanical loading with both isothermal and cyclic thermal loading will be examined. Candidate materials 304 stainless steel, IN617, DS GTD-111 and Ti6242S were chosen due to their diversity in creep and fatigue strength as well as their usage in key high value components. For example 304SS is a common alloy used for springs and steam turbine blades. The material IN617, a wrought Ni-based alloy, is useful as a combustor basket material. First and second stage blades are often derived from directionally solidified Ni-based superalloys, like DS GTD-11. Finally, Ti6242S is a structural alloy used in aircraft engines where the high specific strength of titanium alloys are desirable. Developing constitutive models across an ensemble of solids having membership in distinct strength/alloy classes represents a viable approach to ensuring that said constitutive model can be used ubiquitously throughout a device. Available data are used to explore temperature-dependence of a candidate thermoviscoplasticity model.

CHAPTER 2: BACKGROUND

When modeling the time-dependent cyclic deformation behavior of materials, with emphasis on cyclic loading, there are several viscoplasticity models such as those proposed by Miller [4], Robinson [5], Chaboche [6], Bodner [7], Krempl [8], and Walker [9]. These models all predict deformation for isothermal conditions, and require different modeling parameters for each temperature [10]. In many instances, the model parameters are optimized to regress completely-reversed cyclic data at high temperatures. While these models do not inherently incorporate a temperature-dependent term, it is possible to apply a temperature-dependence by making the parameters used in each model a function of temperature.

2.1 Chaboche Viscoplasticity

The Chaboche model features a von Mises yield criterion given by [11]

$$\sigma_v = |\sigma - \chi| - R \tag{1}$$

where σ_v is the von Mises stress in MPa or ksi, σ is the current stress value, χ is the kinematic hardening, and R is the isotropic hardening. If the von Mises stress exceeds the yield stress, then the material yields. This is suitable for isotropic materials due to its equal yield criterion in both compression and tension prior to kinematic hardening. Hooke's law is given by [11]

$$\sigma = E\varepsilon_{el} \tag{2}$$

where E is the is the Young's Modulus which is a property of the material with units of MPa and ε_{el} is the elastic strain, is used to calculate the stress based off the elastic strain or vice versa. The

total strain can be broken into both the elastic component used in Hooke's law, which contributes to stress, and inelastic strain via [12]

$$\varepsilon = \varepsilon_{el} + \varepsilon_{in} \tag{3}$$

In order to calculate the inelastic strain it is necessary to utilize a flow rule. The form used with the Chaboche model utilizes the von Mises yield criterion and is given in uniaxial form by the following [6]

$$\dot{\varepsilon}_{in} = \langle |\sigma - \chi| - R - k \rangle \left(\frac{\sigma - \chi - R - k}{D} \right)^n \tag{4}$$

where Z is the drag stress, which is a material property with units of $MPa\,s^{1/n}$, n is an exponential term which is a unitless material property, $\dot{\varepsilon}_{in}$ is the inelastic strain rate and $\langle f \rangle$ are the Macaulay Brackets of f. If $f \leq 0$ then the material behaves elastically and follows Hooke's Law and if $f > 0$ then the material behaves plastically.

2.2 Internal State Variables

Internal state variables capture the history, rate, evolution of properties, and other behavior necessary to track the response of a material. Both the kinematic hardening, χ, and the isotropic hardening, R, act as internal state variables in the Chaboche model. This means that knowing the loading history of a material is essential to properly modeling it as numerous values for both variables can exist at a given state depending on how the component was loaded.

The kinematic hardening, which acts as a back stress, acts to move the yield surface which allows for directional hardening [10]. This means that with kinematic hardening the material will

exhibit asymmetric yield strength with a higher yield in either tension or compression depending on the value of the kinematic hardening. The kinematic hardening develops during the plastic deformation of the material. Many different forms of kinematic hardening exist, including linear but one of the more common types is the Armstrong-Frederick non-linear kinematic hardening rule given in uniaxial form [11], i.e.,

$$\dot{\chi}_i = C_i(a_i\dot{\varepsilon}_{in} - \chi_i\dot{p}) \tag{5}$$

where $\dot{\chi}_i$ is the kinematic hardening rate, $\dot{\varepsilon}_{in}$ is the inelastic strain rate, χ_i is the kinematic hardening, $\dot{p}$ is the accumulative inelastic strain rate, C_i is a unitless material constant, and a_i is a material constant with units of MPa. The accumulative plastic strain rate is given by [12]

$$\dot{p} = \left|\dot{\varepsilon}_{in}\right| \tag{6}$$

and the kinematic hardening is given by [12]

$$\chi = \sum_{i=1}^{j} \chi_i \tag{7}$$

where j is the number of kinematic hardening terms. Any number of kinematic hardening terms can be used to increase the model performance, as each kinematic hardening term provides two additional constants in the model that can be varied. Adding these additional constants, however, is often unnecessary to fit the data and adds increased complexity. Two or three kinematic hardening terms are typically used [11, 12, 13, 14]. A visual representation of how linear and non-linear kinematic hardening laws, such as the Armstrong-Fredrick type, affect the yield surface is shown in Figure 2, with the lines depicting the movement of the yield surface.

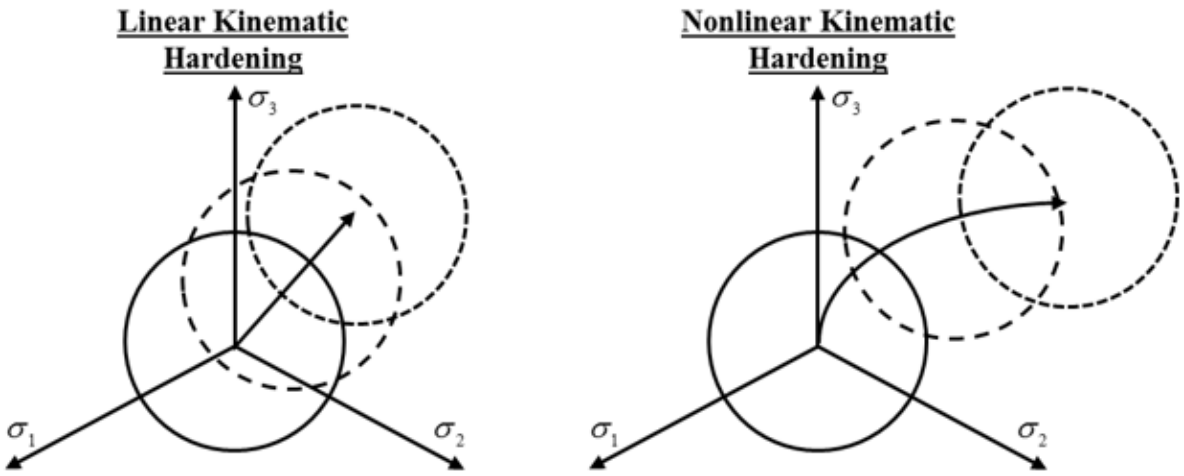

Figure 2: Comparison of the effects of linear and nonlinear kinematic hardening on the yield surface

Isotropic hardening allows for the expansion or contraction of the yield surface, depending on if the material exhibits cyclic hardening or softening behavior respectively, with increased cycles as seen in Figure 3[10]. When isotropic hardening is employed, the stress range will change incrementally with each cycle. Hardening is characterized by the increase of flow stress with cyclic plasticity, and softening is characterized by a decrease. As is the case with kinematic hardening, numerous forms of isotropic hardening rules exist. One commonly used form is a nonlinear isotropic hardening given by [11]

$$\dot{R} = b(Q - R)\dot{p} \tag{8}$$

where $\dot{R}$ is the isotropic hardening rate and Q and b are material constants [11]. A visual representation of the effects of both linear and nonlinear isotropic hardening on the yield surface is shown in Figure 3.

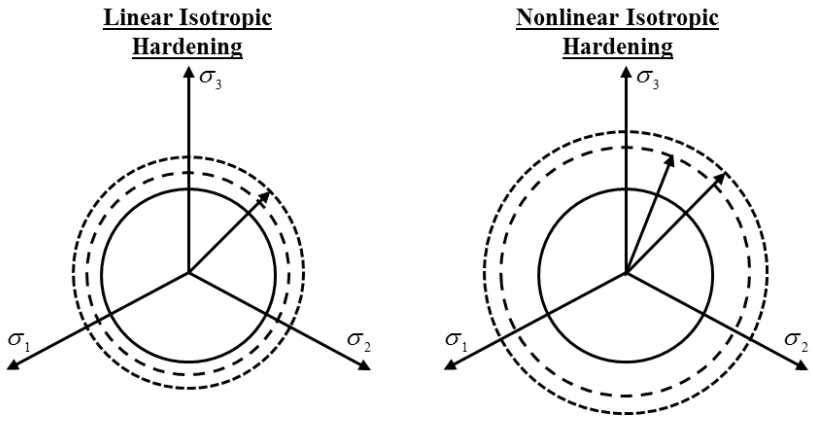

Figure 3: Comparison of the effects of linear and nonlinear isotropic hardening on the yield surface

The Chaboche model, as presented, can contain anywhere from 8 to 14 constants depending on the kinematic hardening formulation. Plasticity methods have not progressed to the level needed to achieve the constants analytically. As a consequence, heuristic methods are used to initialize the constants (discussed in section 2.3) and numerical methods are employed to optimize them (see section 2.4). In both cases, deformation data are needed.

2.3 Initial Parameter Estimation Approach

Incorporating all of these rules leads a large number of constants, ten when using two kinematic hardening terms, to be determined. Traditionally, these constants are found for a material using cyclic isothermal tests. Methods for determining these constants have been outlined in papers such as those by Gong [12], Tong [13], Brommesson [14], and Schwertel [15]. These methods involve finding initial values for the isotropic hardening and kinematic hardening constants, as well as the drag stress and exponential terms and then refining them by means of a numerical optimization code to refine them. The initial elastic modulus is typically determined analytically via a tensile test or the first quarter cycle of a cyclic test by fitting a linear regression

to the linear portion of the stress-strain curve. The initial yield stress is found by identifying the point where the stress-strain curve deviates from linear behavior, known as the proportional limit [12,13].

The isotropic hardening constants are determined from the change in stress amplitude and the accumulated plastic strain between cycles in a fully reversed strain-controlled isothermal fatigue test. Integrating Eq. 8 with respect to time gives

$$R = Q(1 - e^{-bp}) \tag{9}$$

which shows that R will approach a maximum value, Q [12,13]. The accumulated plastic strain, p, can be determined by adding the plastic strain range of each cycle. If it is assumed that the kinematic hardening does not contribute to the change in stress range between cycles, then it can be assumed that it is all from isotropic hardening. Using this a plot like that in Figure 4 [12] can be used to determine Q by looking for the value the plot approaches in later cycles. The other isotropic hardening parameter, b, can be found by choosing a point in the transient region and solving Eq. 9 for b.

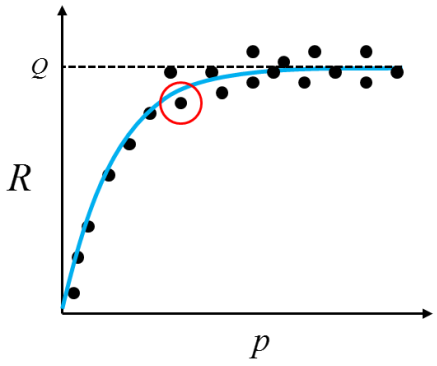

Figure 4: Plot of isotropic hardening vs. accumulated plastic strain [12]

The initial kinematic hardening constants are found from an isothermal tensile test or the first quarter cycle of an isothermal cyclic test. Integrating the equation for the kinematic hardening rate with respect to time gives the equation

$$\chi_i = a_i \left(1 - e^{-C_i \varepsilon_p}\right) \tag{10}$$

which when plugged into the flow rule for the first quarter cycle gives

$$\sigma = a_1(1 - e^{-C_1 \varepsilon_p}) + a_2(1 - e^{-C_2 \varepsilon_p}) + R + k + \sigma_v \tag{11}$$

If it is assumed that the first kinematic hardening term will contribute to most of the kinematic hardening in the early part of the quarter cycle, and the second kinematic hardening term will contribute to most of the kinematic hardening in the later part of the quarter cycle then it is possible to rearrange the equation, differentiate the equation with respect to ε_p, and take the natural logarithm to obtain the following:

$$\ln\left(\frac{\partial \sigma}{\partial \varepsilon_p} - \frac{\partial R}{\partial \varepsilon_p}\right) = -C_i \varepsilon_p + \ln(a_i C_i) \tag{12}$$

which allows for C_1 and C_2 from the slope of a linear regression fit to a plot of the left hand side of Eq. 12 versus ε_p for the early portion and late portion of the first quarter cycle respectively. The other two kinematic hardening parameters, a_1 and a_2, can be found from the ordinate-intercepts of these regressions [12,13]. An example of this type of plot is shown in Figure 5 [12].

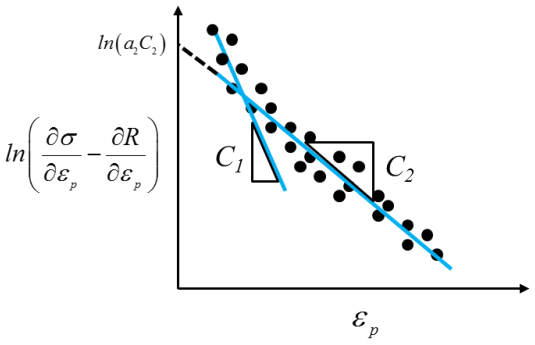

Figure 5: Plot used to determine kinematic hardening parameters [12]

Based on these methods certain parameters are best determined by different tests. An outline of which tests are best for determining each constant can be seen in Table 1. In the cases where monotonic tests are used the first cycle of a cyclic test can be used in its place. Monotonic tests can be used to determine the elastic modulus, proportional limit, and kinematic hardening terms. It is necessary to have cyclic tests in order to determine the isotropic hardening.

Table 1: Outline of which tests can be used to determine material properties

Material Properties	Test Used to Determine
E (MPa), Elastic Modulus	Monotonic
k (MPa), Proportional Limit	Monotonic
a_1 (MPa), Kinematic Hardening Term	Monotonic
a_2 (MPa), Kinematic Hardening Term	Monotonic
C_1, Kinematic Hardening Term	Monotonic
C_2, Kinematic Hardening Term	Monotonic
Q (MPa), Isotropic Hardening Term	Cyclic
b, Isotropic Hardening Term	Cyclic
Z ($MPa * s^{1/n}$) , Drag Stress	Monotonic
n, exponential term	Monotonic

2.4 Parameter Optimization

After the initial constants are found, they are typically given to an optimization routine [12,13]. This routine usually optimizes all of the constants and is done in a software such as MATLAB. A flowchart that shows how these optimization routines typically work can be seen in Figure 6 [12].

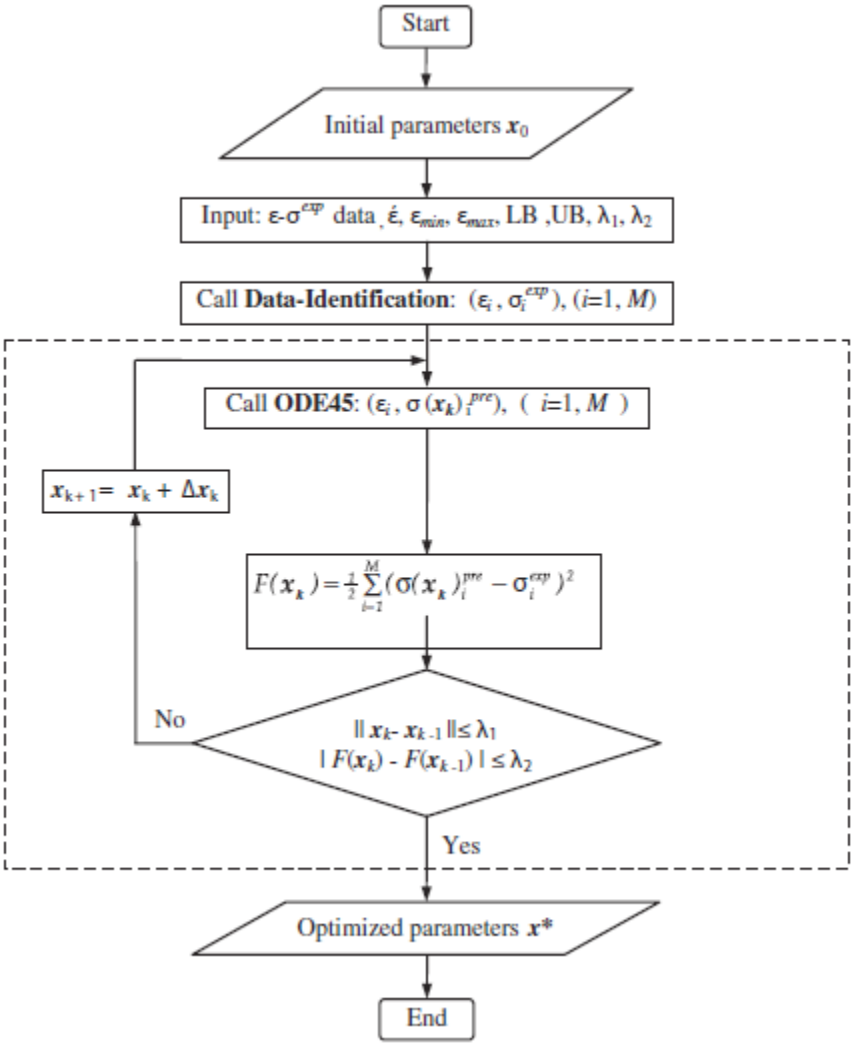

Figure 6: Flowchart of a typical optimization code for material properties [12]

In order to accurately model non-isothermal loadings, it is necessary to have a method for finding constants at intermediate temperatures where no data is available. Linear interpolation for all temperature-dependent constants is the most common way of finding these constants. This method of modeling non-isothermal loadings has demonstrated the ability to achieve a reasonable fit [16]; however, it is unlikely that all of the temperature-dependent parameters exhibit this behavior. Another investigation into adding temperature-dependence to the Chaboche model employed using an Arrhenius-type temperature effect [17], i.e.,

$$K(T) = k_1 \exp(\frac{-k_2}{T}) \tag{13}$$

where *K(T)* is a multiplier of the flow rule given in Eq. 4, *T* is the temperature, and k_1 and k_2 are material constants. This was shown to work well over a narrow range of temperatures [17]. Neu examines the temperature-dependence of parameters for a different unified constitutive model using a titanium alloy [18] and Karl examines life prediction techniques for 304 stainless steel using damage based and phenomenological models [19]. There have also been investigation to adding temperature-dependence to other models. It is also worth noting that many materials show a temperature-rate dependence and methods for modeling this dependence often require smooth and continuous functions for these parameters. Exploration into the temperature-dependence of Chaboche constants is not seen in literature. Furthermore, viscoplasticity modeling of the candidate materials across a wide range of temperatures and comparisons of Chaboche constants across materials have not yet been explored.

The purpose of this research is to determine which mathematical models can be used to better describe these parameters for the candidate materials in order to achieve more accurate thermomechanical fatigue simulations and allow for the addition of temperature-rate dependence into the model. In order to find these mathematical models, isothermal constants will be acquired at a variety of temperatures and math models will be regressed to describe their behavior with respect to temperature.

CHAPTER 3: MATERIALS

The materials examined in this study, namely 304SS, IN617, DS GTD-111, and Ti6242S, have a variety of base materials, strength classes, and applications. The applications of each material along with their chemical composition are outlined in this chapter.

3.1 Stainless Steel 304

Type 304 stainless steel is a widely used alloy with many varied applications. Due to the presence of chromium it offers better oxidation resistance than other steels allowing making it ideal for a wide range of applications. Stainless steel 304 can be seen in many applications from the manufacture of medical devices [20] to repair seals in pipe clamps [21]. Some of its uses subject it to thermomechanical fatigue (TMF) such as in certain turbomachinery components. The chemical composition of 304 stainless steel is shown in Table 2 [22]. The material is nominally 69% iron. It is assumed to be isotropic and has a melting point of 1400°C.

Table 2: Composition of 304 stainless steel in wt%

Element	C	Cr	Mn	Ni	P	S	Si	Fe
Min	-	18	-	8	-	-	-	Bal.
Max	0.08	20	2	10.5	0.045	0.03	1	Bal.

3.2 IN617

Due to its excellent strength and creep resistance at higher temperatures IN617 has seen use in turbine engines, nuclear reactors, and aerospace applications. Its nickel content provide it good tensile strength and fatigue resistance at higher temperatures. The chemical composition of IN617 is shown in Table 3 [23]. It has a melting temperature of 1350°C and a face-centered-cubic (FCC) crystal structure.

Table 3: Composition of IN617 in wt%

Element	Al	B	C	Co	Cr	Cu	Fe	Mn	Mo	Si	Ti	Ni
Min	0.08	-	0.05	10.0	20.0	-	-	-	8.0	-	-	Bal.
Max	1.5	0.06	0.15	15.0	24.0	0.05	3.0	1.0	10.0	1.0	0.6	Bal.

3.3 DS GTD – 111

The directional solidification of materials such as DS GTD-111, a Ni-base superalloy, produces long columnar grains that improve corrosion, creep, thermal fatigue, and impact resistance. Due to the directional solidification, the properties of DS GTD-111 differ depending upon orientation. It is often used in gas turbines. Similar to IN617 it has an FCC structure and a high melting point [24]. Its chemical composition is shown in Table 4 [24].

Table 4: Composition of DS GTD-111 in wt%

Element	Al	B	C	Co	Cr	Cu	Fe	Mn	Mo	P	S	Si	Ta	Ti	W	Zr	Ni
Min	2.8	-	0.08	9.0	13.7	-	-	-	1.4	-	-	-	2.5	4.7	3.5	0.005	Bal.
Max	3.2	0.020	0.12	10.0	14.3	0.1	0.35	0.1	1.7	0.015	0.015	0.3	3.1	5.1	4.1	0.040	Bal.

3.4 Ti6242S

The titanium alloy Ti6242S exhibits good creep and fatigue resistance at temperatures of up to 500°C. This combined with its low density makes the material suitable for aerospace applications. The chemical composition of Ti6242 is shown in Table 5 [25]. It has a melting point of 1700°C.

Table 5: Composition of Ti6242S in wt%

Element	Al	C	H	Fe	Mo	N	O	Si	Sn	Ti
Min	5.5	-	-	-	1.8	-	-	0.08	1.8	Bal.
Max	6.5	0.05	0.015	0.25	2.2	0.05	0.15	0.1	2.2	Bal.

CHAPTER 4: PARAMETER DETERMINATION

The documented methods of finding parameters for the Chaboche viscoplasticity model work well for achieving fits for isothermal tests; however, they do not typically lead to consistent behavior for many of the parameters across temperatures. In order to allow for modeling of TMF loadings, it is necessary to modify these techniques.

4.1 General Parameters

The Chaboche viscoplasticity model and associated ISVs (shown in Eqs. 4-8), as implemented in this research requires ten parameters. The elastic modulus, E, can be found from the slope of the linear portion of either a monotonic test or the first quarter cycle of a cyclic test, as shown in Figure 7. In the case of a cyclic test it can also be found from the linear portion after a reversal in the direction of the change of strain, the point in a test at which the strain switches from increasing to decreasing or vice versa.

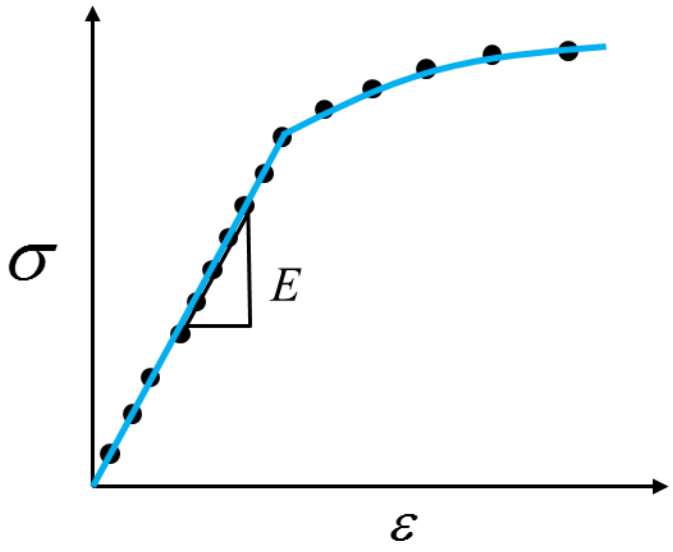

Figure 7: Example of finding an elastic modulus from data

The yield stress, k, can also be easily found from a monotonic test. There is a desire for an analytical method to find this value to allow for repeatable results. While typically this is done by finding the point where a line with a slope equal to the elastic modulus and an x-intercept of 0.2% strain intersects the monotonic test, since the yield stress acts as the proportional limit this tends to extend the linear portion of the curve much too far. As a result an offset of 0.01% was used instead. An example of this is shown in Figure 8. The red circle where the line and blue curve intersects represents the yield stress.

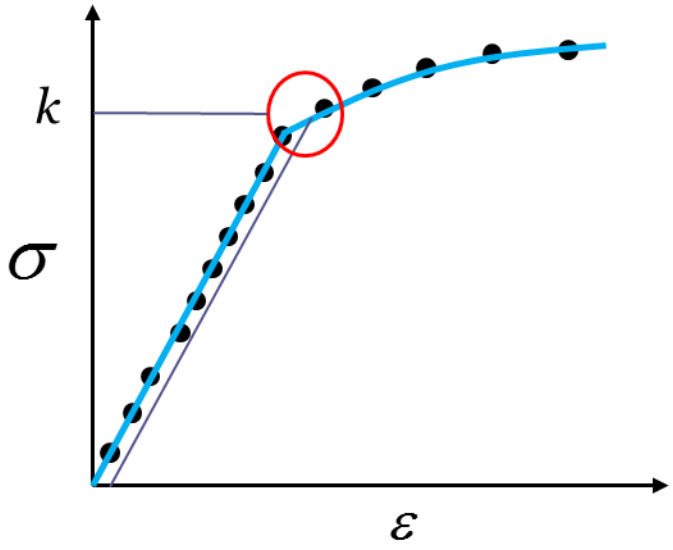

Figure 8: Example of finding the 0.01% offset yield stress

Once initial values of all of the parameters have been developed it is typical to run them through a numerical optimization routine [12, 13]. A flowchart of the numerical optimization routine, implemented in MATLAB, used for this research can be seen below in Figure 9. It utilizes the built in MATLAB function *fminsearch* which searches for the constants that provide a minimum in the error [26]. The error is defined as

$$Err = \sum_{i=1}^{m} \left(\sigma_c^{(i)} - \sigma_{\exp}^{(i)} \right)^2 \tag{14}$$

where *err*, is the error, $\sigma_c^{(i)}$ is the stress calculated using the Chaboche viscoplasticity model, and $\sigma_{\exp}^{(i)}$ is the stress value of the data. In order to avoid interpolation for this error calculation, a stress was calculated at each of the strain points for the test data.

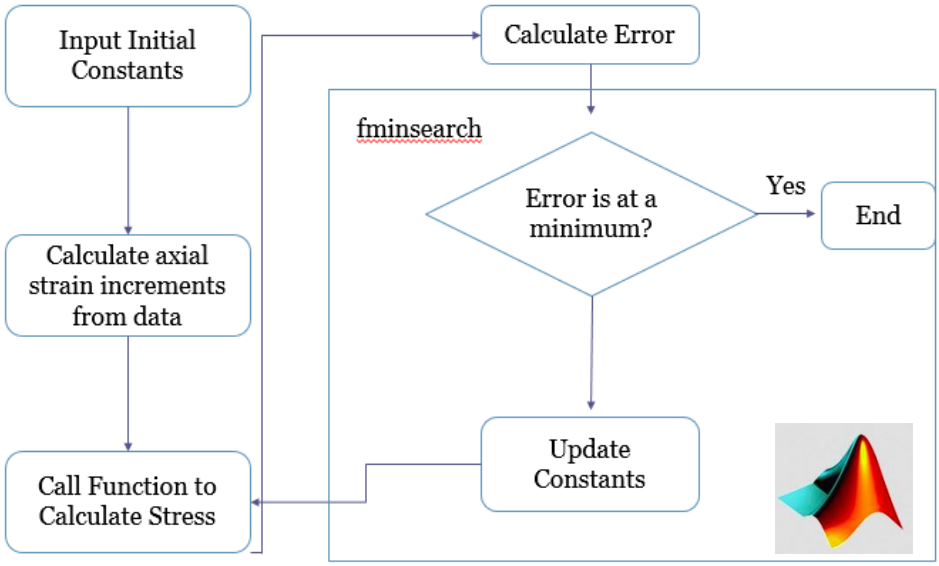

Figure 9: Flowchart of MATLAB optimization routine

While it is common to run all ten parameters through the optimization code this can lead unnecessarily long run times for the optimization code and, in some cases, lead to a wide variation in the parameters seen between temperatures. For example the constants for 316 stainless steel found by Gong, as shown in Table 6, seem to show no clear behavior for parameters other than *k* and *E* [12].

Table 6: Constants for 316 stainless steel found by Gong [12] at various temperatures

T (°C)	k (MPa)	E (MPa)	b	Q (MPa)	a_1 (MPa)	C_1	a_2 (MPa)	C_2	Z (MPa.s$^{1/n}$)	n
300	28.99	159.066	19.92	26.79	55.47	16343.09	211.22	1215.4	116.06	7.21
500	37.98	135.467	16.77	32.79	36.66	19963.66	160.59	1506.58	70.6	40
550	27.29	146.936	11.29	36.93	70.17	11744.56	171.01	1396.05	39.72	11.38
600	18.98	149.69	42.45	28.68	87.56	7285.09	163.53	1328.7	129.12	3.72

Since both the elastic modulus and the yield stress are well defined values that can easily be found analytically, they were not run through the optimization code. In order to ensure consistent behavior for parameters across a range of temperatures, holding certain parameters constant proved effective. It was seen that there were enough constants to be able to hold Z and n constant without adversely affecting the ability to fit data as will be seen in chapter 5. Furthermore, it resulted in more consistent behavior with respect to temperature for the other parameters.

4.2 Kinematic Hardening

After finding optimized constants for isothermal tests at available temperatures, the parameters were examined for trends. In the event that the kinematic hardening constants had many inflection points with changing temperature, C_1 and C_2 where designed so that they would produce a smoother curve when plotted against temperature and allow for a more simple math model to fit the isothermal values found for the constants. The values for a_1 and a_2 were then iterated through the optimization routine again with the new values for C_1 and C_2 held constant. This allowed for more consistent behavior with changing temperature for all kinematic hardening constants.

4.3 Isotropic Hardening

For the isotropic hardening a similar method to that used with the kinematic hardening was employed. In the event that the parameter Q showed unexpected inflection points, it would be

designed to get rid of the inflection points, and then *b* would be optimized with the new value for *Q* held constant. Once again, this allowed for more consistent behavior with changing temperature, which allowed for fitting better behaved math models.

CHAPTER 5: MODELING

The four candidate materials were compared to available data at various temperatures. The constants were then found for each material using the methods described above. The resulting curves are shown in this section.

5.1 Isothermal LCF

For 304 stainless steel, low cycle fatigue (LCF) data was available at 200°C and 600°C. Both of these tests were conducted at a strain rate of $1.0e-3\ s^{-1}$ with strain ranges of 1.4%. The fit for the 200°C data can be seen in Figure 10 and the fit for the 600°C data can be seen in figure Figure 11. Good fits were obtained for both temperatures, with some amount of tensile compressive asymmetry that wasn't captured due to the von Mises yield criterion

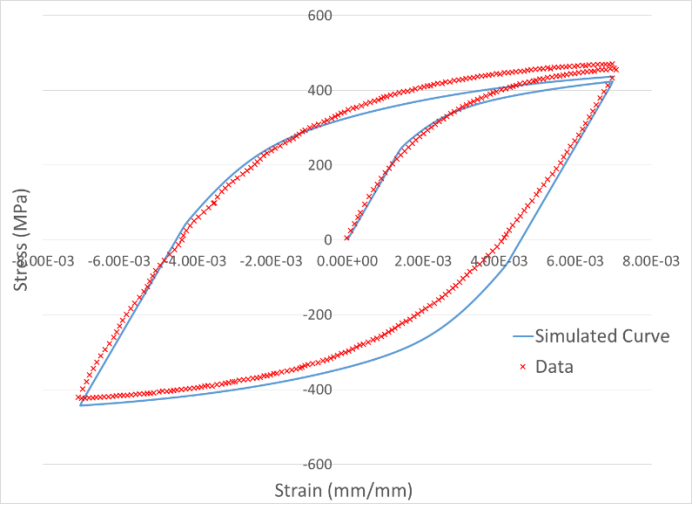

Figure 10: Comparison of data and simulated curve for 304SS at 200°C

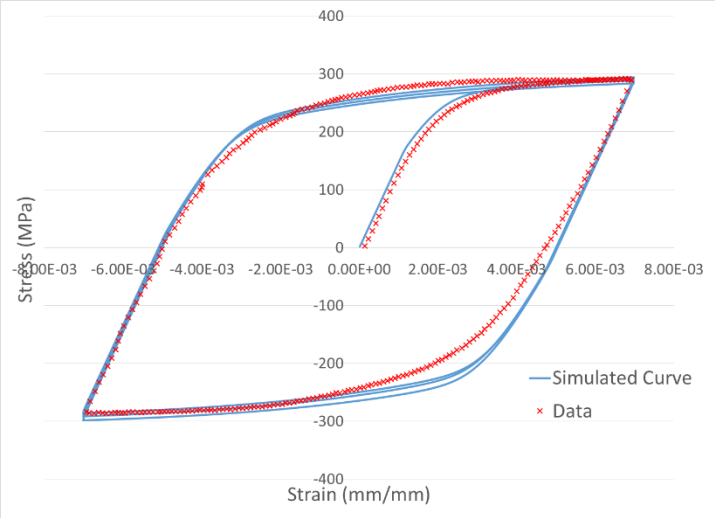

Figure 11: Comparison of data and simulated curve for 304SS at 600°C

For IN617 the data was fit to fully reversed simulated data based on the Ramberg-Osgood constants available at various temperatures. This meant that isotropic hardening had to be ignored for this data, as there was no cyclic data from which to obtain values for the parameters. Comparisons of these are shown below in Figure 12-Figure ***18***. For all temperatures the plastic strain range was calculated very accurately. For the most part, the stress was calculated well with some variation upon initial yielding seen in the temperatures between 648°C and 815°C.

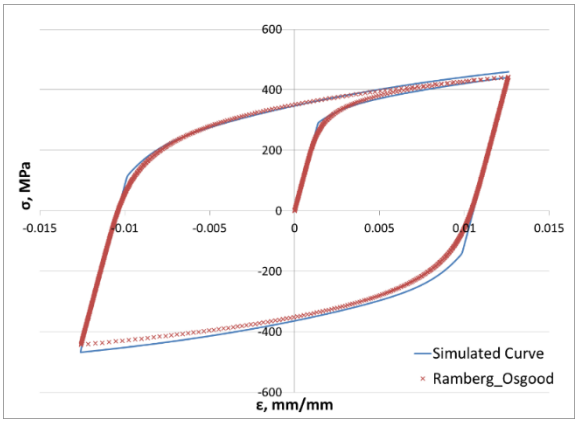

Figure 12: Comparison of Ramberg-Osgood and Simulated curves for IN617 at 21°C

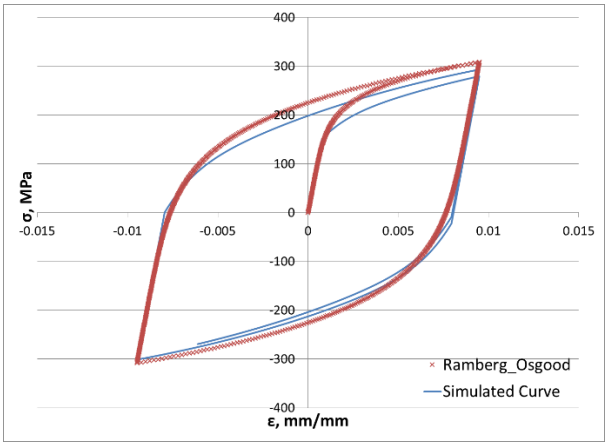

Figure 13: Comparison of Ramberg-Osgood and Simulated curves for IN617 at 287°C

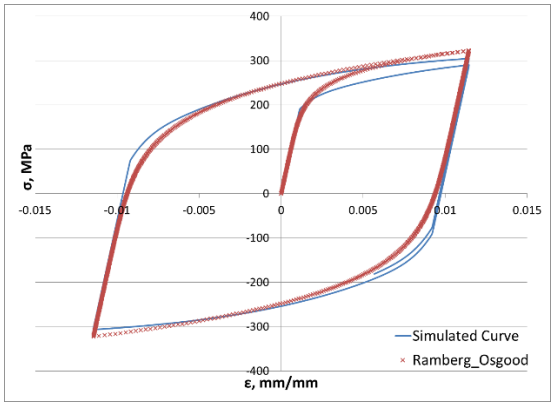

Figure 14: Comparison of Ramberg-Osgood and Simulated curves for IN617 at 648°C

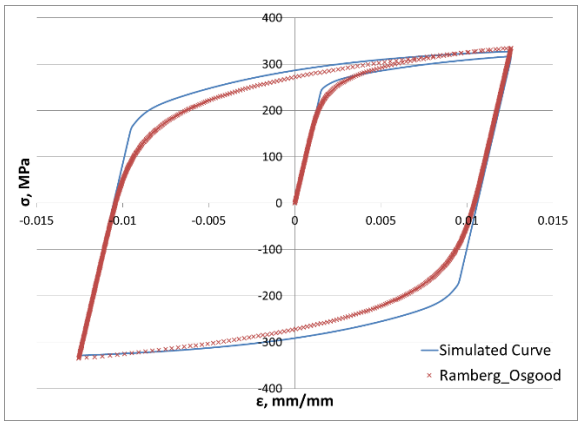

Figure 15: Comparison of Ramberg-Osgood and Simulated curves for IN617 at 760°C

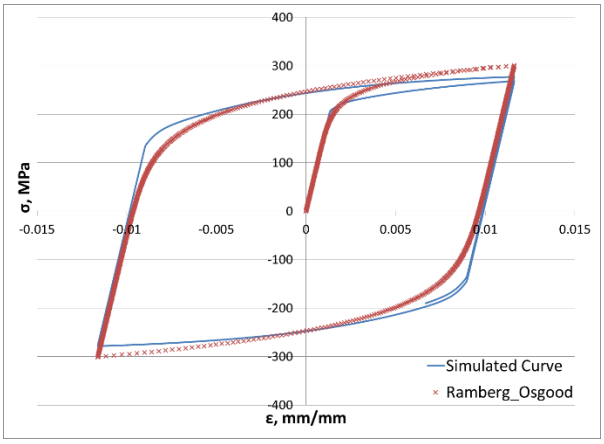

Figure 16: Comparison of Ramberg-Osgood and Simulated curves for IN617 at 815°C

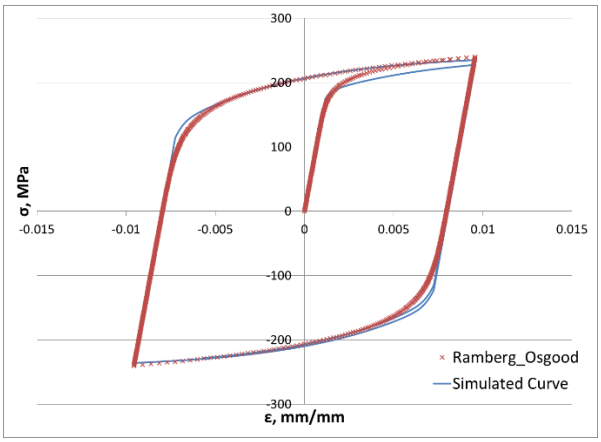

Figure 17: Comparison of Ramberg-Osgood and Simulated curves for IN617 at 871°C

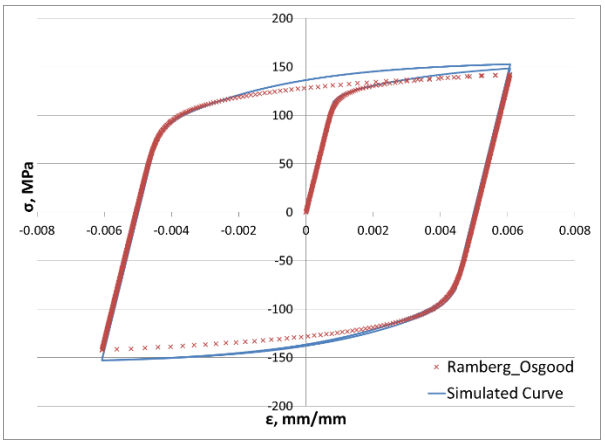

Figure 18: Comparison of Ramberg-Osgood and Simulated curves for IN617 at 982°C

For Ti6242S the same methods were used with fitting the constants to simulated Ramberg-Osgood curves. Once again since there was no cyclic data available, the isotropic hardening was turned off. The comparisons of these curves are shown in Figure 19-Figure ***25***. The plastic strain range was predicted well for all temperatures. The stress range was predicted well for all temperatures, with the exception of some variation seen at 371°C

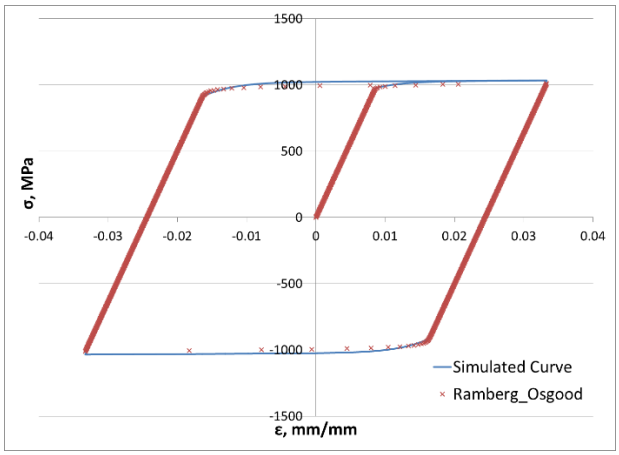

Figure 19: Comparison of Ramberg-Osgood and Simulated curves for Ti6242S at 21°C

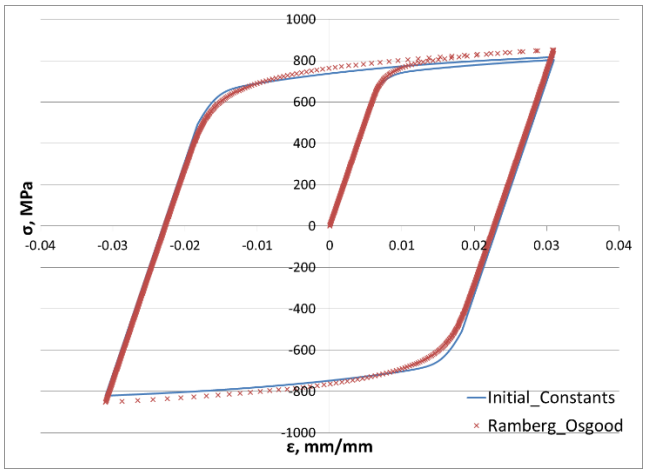

Figure 20: Comparison of Ramberg-Osgood and Simulated curves for Ti6242S at 204°C

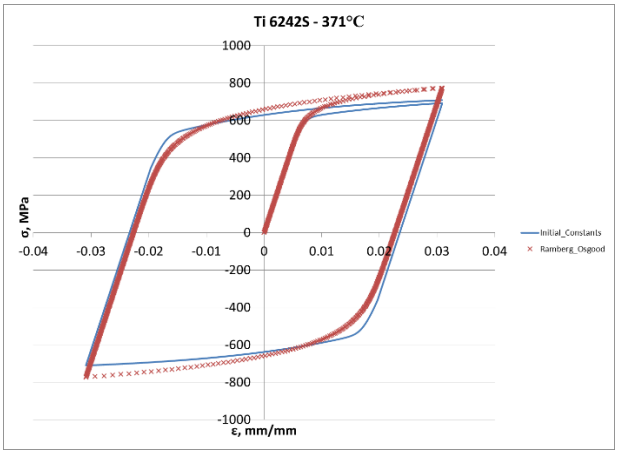

Figure 21: Comparison of Ramberg-Osgood and Simulated curves for Ti6242S at 371°C

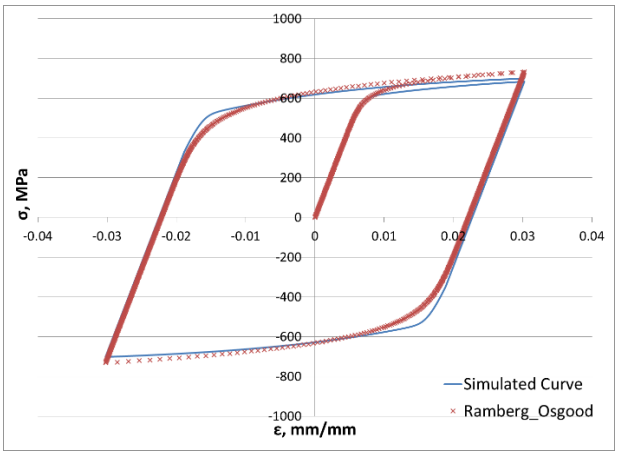

Figure 22: Comparison of Ramberg-Osgood and Simulated curves for Ti6242S at 426°C

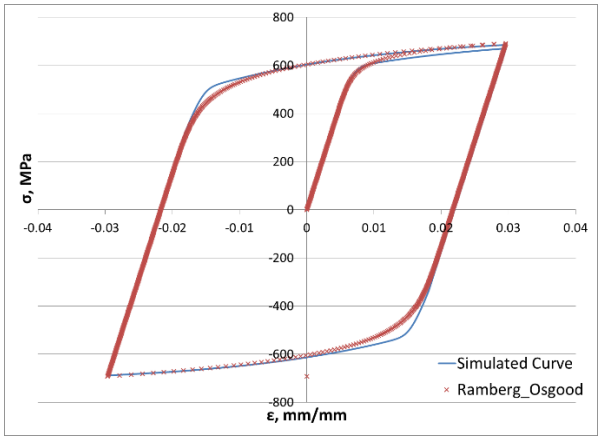

Figure 23: Comparison of Ramberg-Osgood and Simulated curves for Ti6242S at 482°C

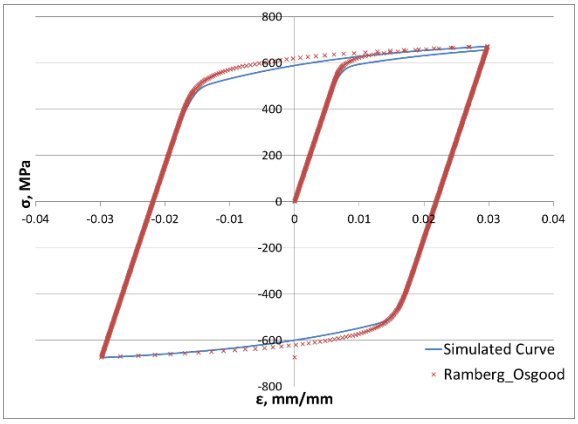

Figure 24: Comparison of Ramberg-Osgood and Simulated curves for Ti6242S at 537°C

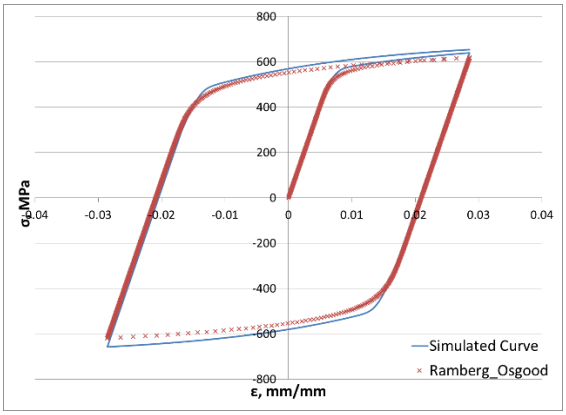

Figure 25: Comparison of Ramberg-Osgood and Simulated curves for Ti6242S at 593°C

For DS GTD-111 data was only available at 871°C; however, the primary interest here was determining the dependence of orientation in directionally solidified materials. In trying to find a set of constants, it was determined that kinematic hardening constants could be held the same across orientations, while isotropic hardening constants had to be different. The fits for DS GTD-111 in both the L and T orientation are shown below in Figure 26 and Figure 27 respectively.

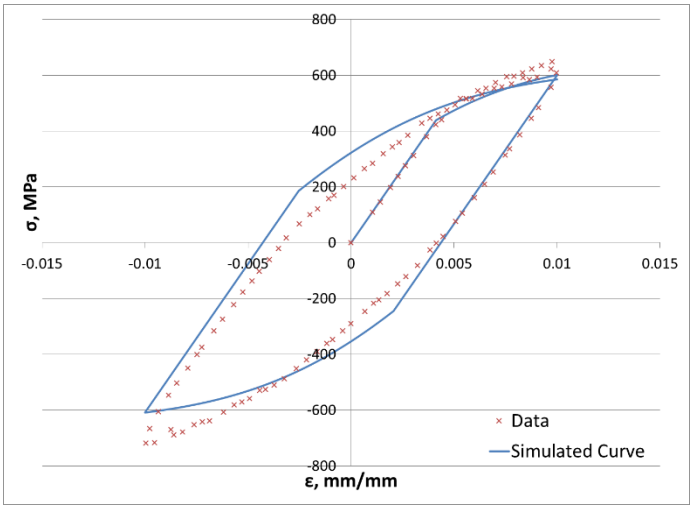

Figure 26: Comparison of data and simulated curve for DS GTD-111 in the L-orientation

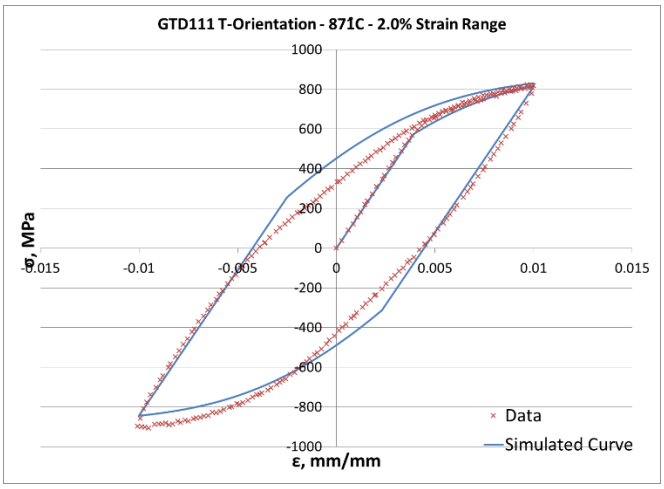

Figure 27: Comparison of data and simulated curve for DS GTD-111 in the T-orientation

5.2 Non-isothermal Fatigue

For 304 stainless steel there were data available for a TMF loading case [19]. Both linear interpolation methods, as well as more complex math models were compared to this data. The results of both are shown in Figure 28. In the case of the non-linear models, power laws were used to define C_1 and C_2. It can be seen from the figure that deviating from linear interpolation provides

a better fit to the data in this case. If there were more isothermal data points available for this material, it would be possible to better define the math models used in this simulation.

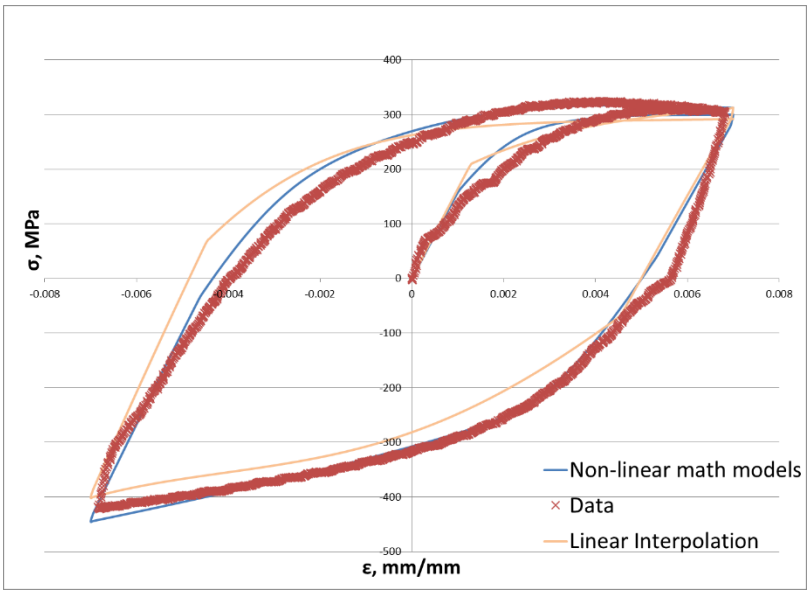

Figure 28: Comparison of data and curves simulated by linear interpolation and non-linear math models for Chaboche parameters of 304 stainless steel

CHAPTER 6: TEMPERATURE EFFECTS

Due to the wide range of temperatures for which there is data available, the temperature dependence of the Chaboche parameters was looked at extensively for IN617 and Ti6242S. In the case of Ti6242S a good fit could be achieved using a linear regression, while for IN617 it was necessary to use a parabolic fit. The plot of elastic modulus with respect to temperature is shown in **Figure *29*** for IN617 and **Figure *30*** for Ti6242S.

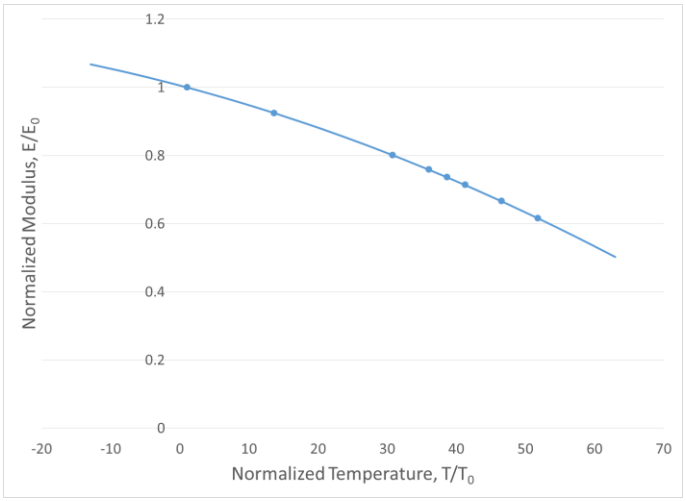

Figure 29: Elastic modulus behavior with respect to temperature for IN617

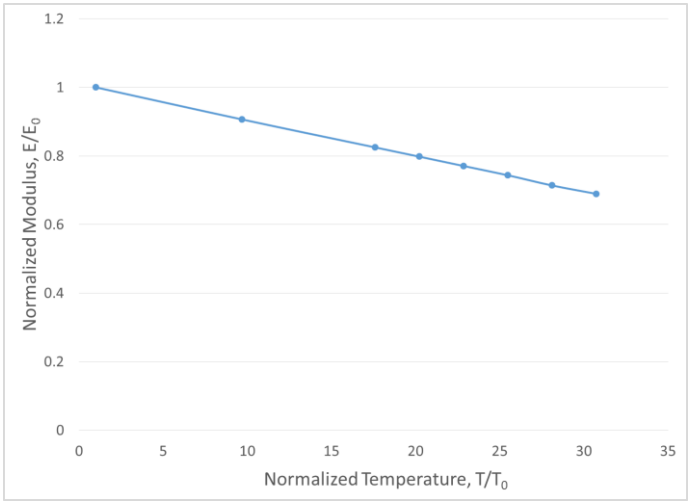

Figure 30: Elastic modulus behavior with respect to temperature for Ti6242S

The yield stress for IN617 exhibits a linear downward pattern until it reaches a value at which point the behavior is parabolic. This is expected of this material, however, as there is a phase shift that causes the yield strength to rise with rising temperatures over certain ranges, which is consistent with the yield strength of IN617. The yield strength of Ti6242S follows a power law.

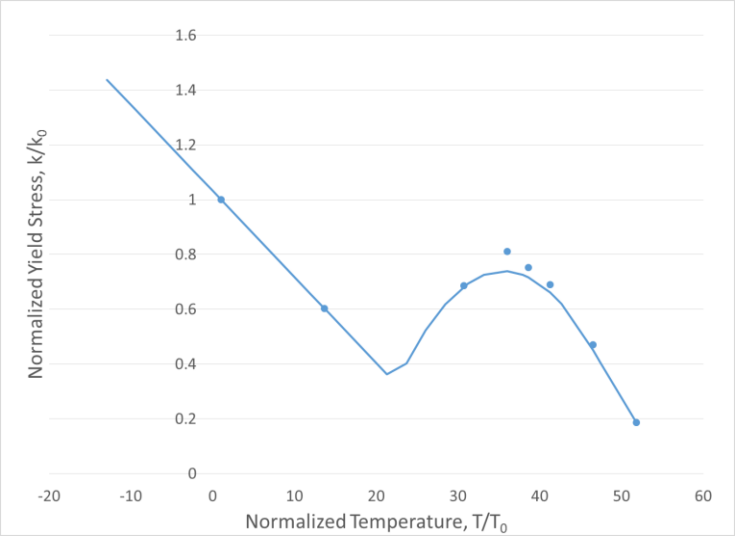

Figure 31: Yield stress behavior with respect to temperature for IN617

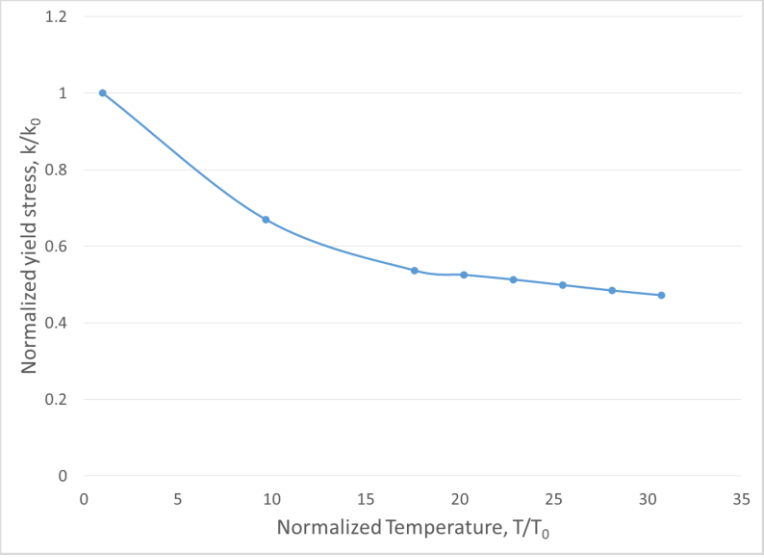

Figure 32: Yield stress behavior with respect to temperature for Ti6242S

The C1 parameter for IN617 follows an exponential law, as seen in **Figure *33***. The behavior of C2, **Figure *34***, follows a linear model over the same temperatures as the yield stress, and switches to a parabolic model. The phase shift again explains why this would occur. The C1 and C2 parameters for Ti6242S follows a power law, as seen in Figure 35 and **Figure *36*** respectively.

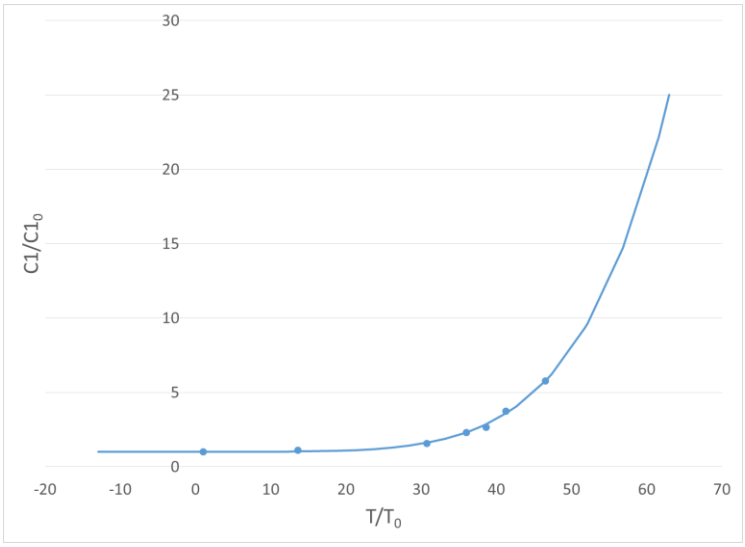

Figure 33: Behavior of C1 with respect to temperature for IN617

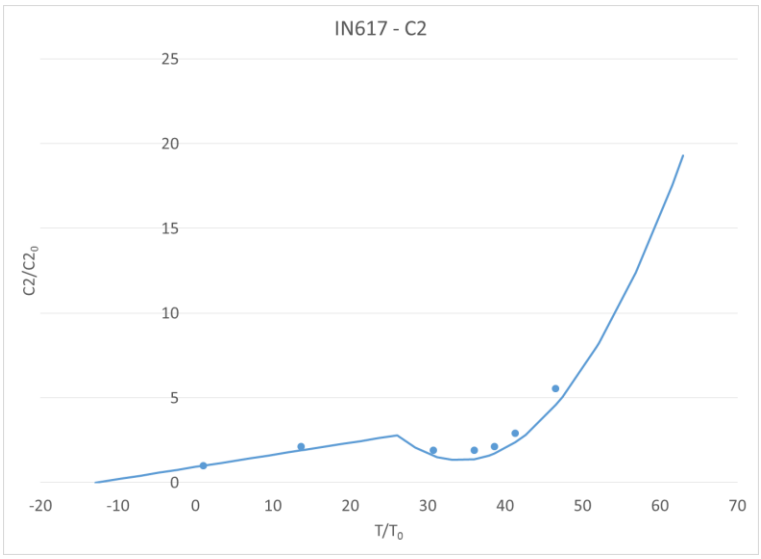

Figure 34: Behavior of C2 with respect to temperature for IN617

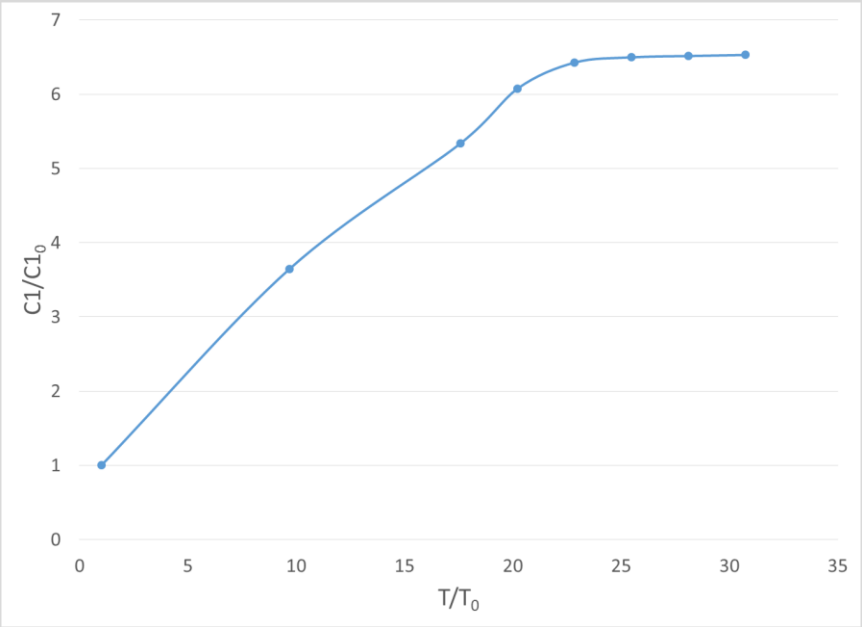

Figure 35: Behavior of C1 with respect to temperature for Ti6242S

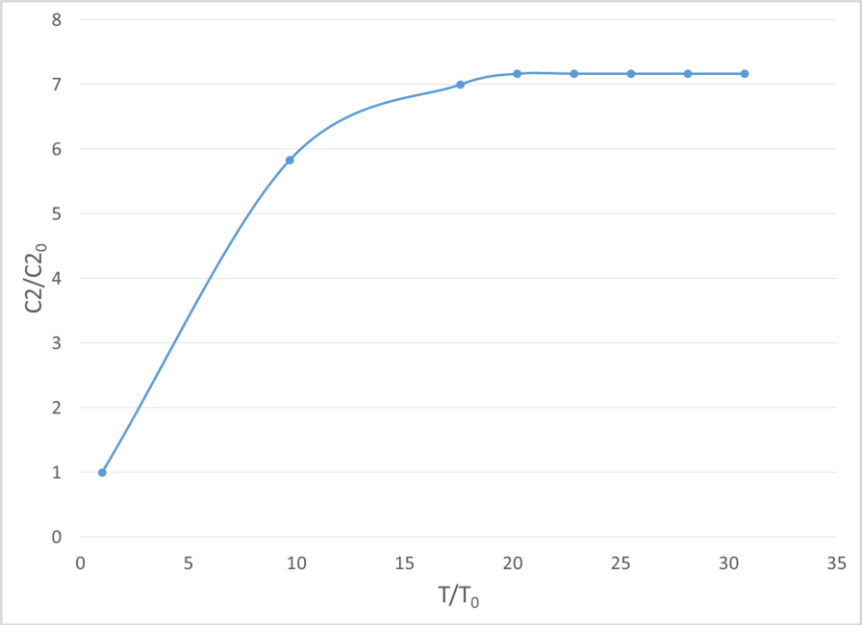

Figure 36: Behavior of C2 with respect to temperature for Ti6242S

For IN617 the behavior for both a1 and a2 is linear as shown in Figure 37 and **Figure *38*** respectively. The behavior for a1 and a2 of Ti6242S has a power law relation as shown in **Figure *39*** and **Figure *40*** respectively.

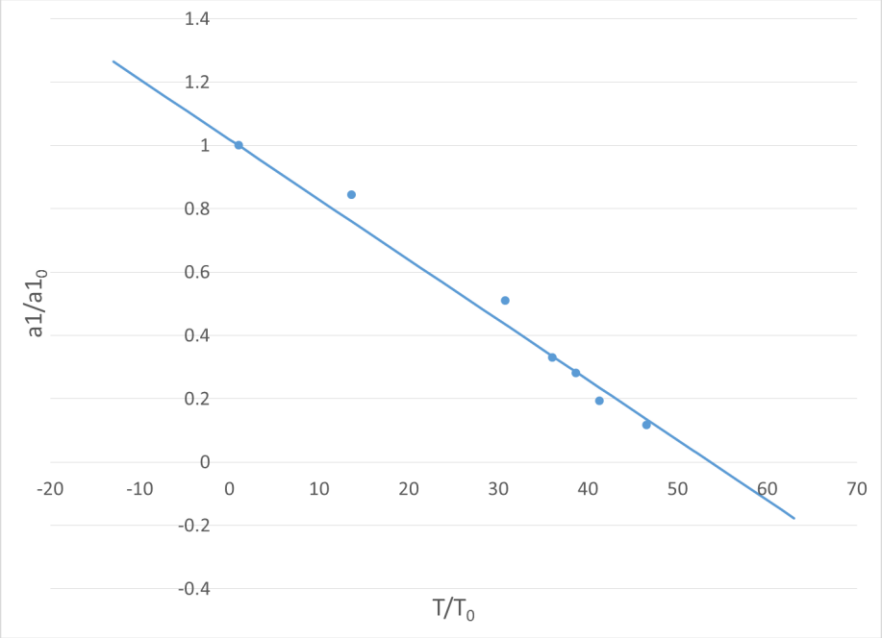

Figure 37: Behavior of a1 with respect to temperature for IN617

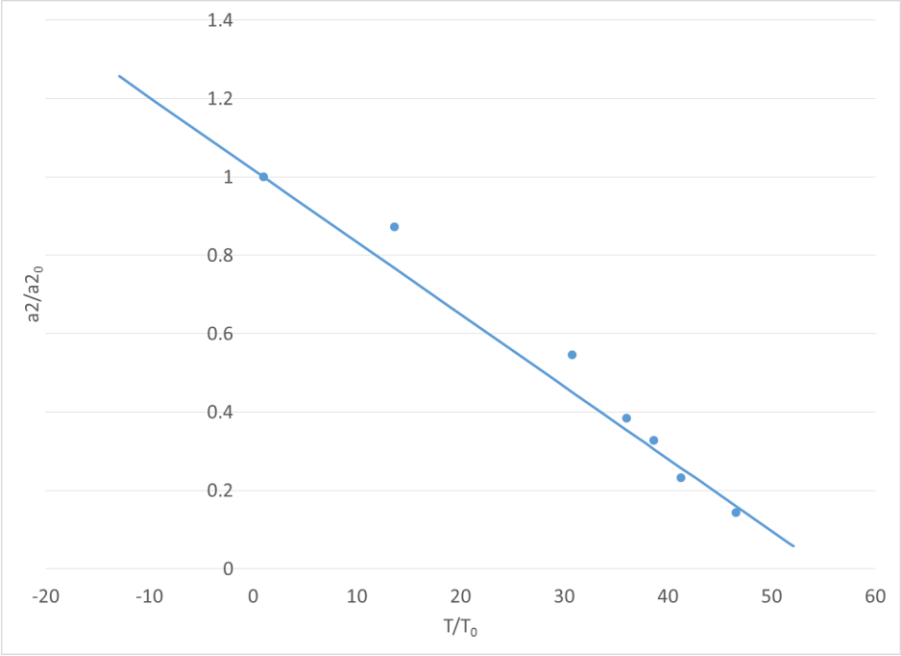

Figure 38: Behavior of a2 with respect to temperature for IN617

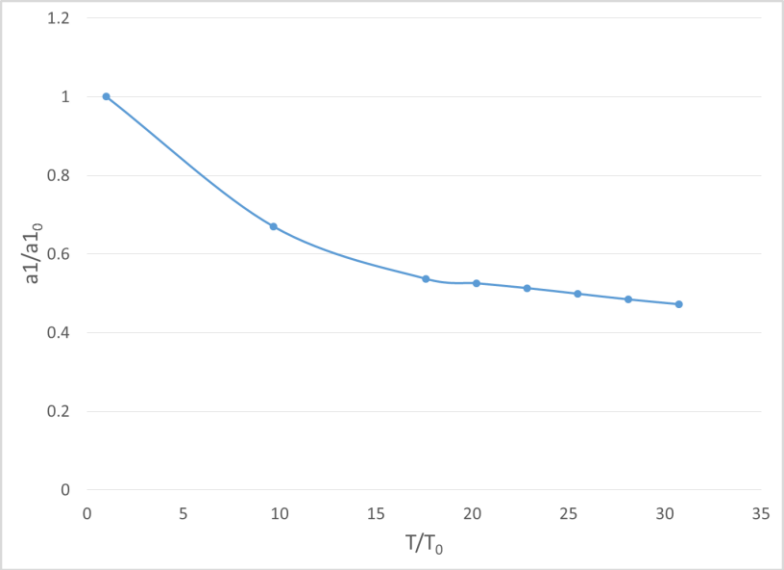

Figure 39: Behavior of a1 with respect to temperature for Ti6242S

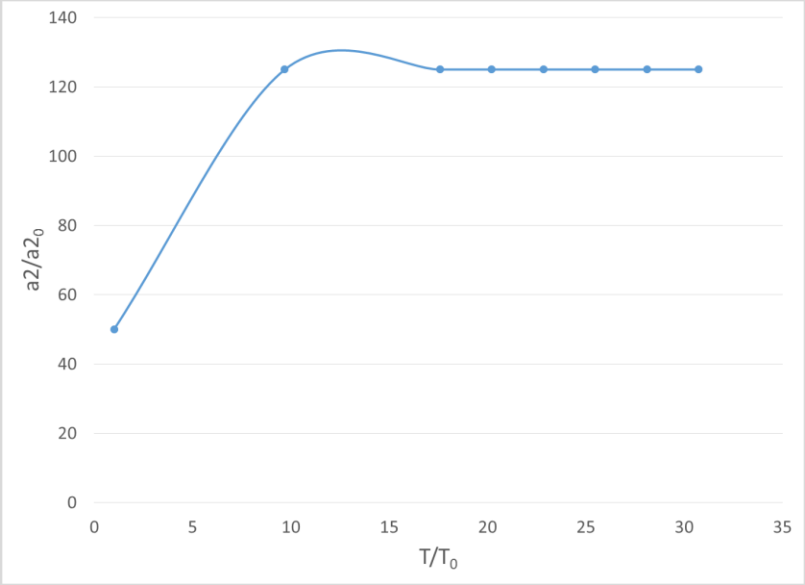

Figure 40: Behavior of a2 with respect to temperature for Ti6242S

CHAPTER 7: CONCLUSIONS

The goal of this research is to provide a method for obtaining better results simulating non-isothermal loading using the Chaboche viscoplasticity model. By utilizing a unique method of optimizing parameters, developed in the present work, it is possible to obtain consistent behavior of material properties with changing temperature. This consistent behavior helps to find mathematical models to describe each parameter, which in turn allows for more accurate results in non-isothermal loadings. As the behavior of the various Chaboche parameters becomes better known, it will be possible to achieve accurate modeling for TMF loadings with far fewer test results than current linear interpolation methods. The methods can be observed to perform satisfactorily for a variety of materials across a number of strength classes. The ability of the model to capture the orientation dependence of a material with Chaboche parameters was also explored in an effort to better understand what behavior to expect for these parameters.

REFERENCES

[1] Zhang, G., Yuan, H., and Li, F., "Analysis of Creep-Fatigue Life Prediction Models for Nickel-Based Super Alloys, "*Computational Materials Science.* Vol. 57, pp. 80-86, 2012.

[2] Steichen, J. M., "Tensile Properties of Thermally Exposed Type 304 Stainless Steel," *Journal of Engineering Materials and Technology.* Vol. 98, No. 4, pp. 357 -360, 1976.

[3] Langston, L., "Crown Jewels," *Mechanical Engineering.* Vol. 128, No. 2, pp. 31-33, 2006.

[4] Miller, A., "An Inelastic Constitutive Model for Monotonic, Cyclic, and Creep Deformation: Part 1. Equations development and analytical procedures," *Journal of Engineering Materials and Technology.* Vol. 98, pp. 97-105, 1976.

[5] Robinson, D. N., "A Unified Creep-Plasticity model for Structural Metals at High Temperature," *ORNL/TM-5969*. 1978.

[6] Chaboche, J.L., "Constitutive Equations for Cyclic Plasticity and Cyclic Viscoplasticity," *International Journal of Plasticity.* Vol. 5, No. 3, pp. 247-302, 1989.

[7] Bodner, S.R., and Partom, Y., "Constitutive Equations for Elastic-Viscoplastic Strain-Hardening Materials," *Journal of Applied Mechanics.* Vol. 42, No. 2, pp. 273-301, 1975.

[8] Krempl, E., Nakamura, T., "The Influence of the Equilibrium Stress Growth Law Formulation on the Modeling of Recently Observed Relaxation Behaviors," *JSME International Journal, Series A: Mechanics and Material Engineering.* Vol. 41, No. 1, pp 103-111, 1998.

[9] Freed, A.D., Walker, K.P., "Model Development in Viscoplastic Ratchetting," *NASA Technical Memorandum 102509,* N90-20431, 1990.

[10] Chaboche, J.L., "A Review of Some Plasticity and Viscoplasticity Constitutive Theories," *International Journal of Plasticity.* Vol. 24, No. 10, pp. 1642 – 1693, 2008.

[11] Dunne, F., and Petrinic, N., 2005. *Introduction to Computational Plasticity*, Oxford. New York. pp. 23-35.

[12] Gong, Y.P., Hyde, C.J., Sun, W., and Hyde, T.H., "Determination of Material Properties in the Chaboche Unified Viscoplasticity Model," *Journal of Materials Design and Applications.* Vol. 224, No. 1, pp. 19-29. 2010.

[13] Tong, J., Zhan, Z. L., and Vermeulen, B., "Modelling of Cyclic Plasticity and Viscoplasticity of a Nickel-Based Alloy using Chaboche Constitutive Equations," *International Journal of Fatigue.* Vol. 26, No. 8, pp. 829-835, 2004.

[14] Brommesson, R., Hörnqvist, M., and Ekh, M., "Low Cycle Fatigue Crack Growth in Ti-6242 at Elevated Temperature," *Advanced Materials Research*. Vols. 891-892, pp. 422-427, 2014.

[15] Schweretel, J., Markling, G., Hornberger, K., and Schinke B., "Experimental Investigations on an Ni-base Superalloy IN617 and Their Theoretical Description," *High Temperature Constitutive Modeling – Theory and Application.* MD-Vol. 26/AMD-Vol. 21, pp. 285-295. 1991.

[16] Hyde, C. J., Sun, W., and Leen, S. B., "Cyclic Thermo-Mechanical Material Modeling and Testing of 316 Stainless Steel," *International Journal of Pressure Vessels and Piping*. Vol. 87, No. 6, pp 365-372, 2010.

[17] Shin, M.J., 1992. *Viscoplastic Constitutive Models for Type 304 Stainless Steel*, Ph.D. Dissertation, University of Missouri-Columbia.

[18] Neu, R.W., "Nonisothermal Parameters for the Bodner-Partom Model," *Material Parameter Estimation for Modern Constitutive Equations*. MD-Vol. 43/AMD-Vol. 168, pp. 211-226, 1993.

[19] Karl, J. O., 2013. *Thermomechanical Fatigue Life Prediction of Notched 304 Stainless Steel,* Ph.D. Dissertation, University of Central Florida.

[20] Zalnezhad, E., Hamouda, A.M.S, Faraji, G., and Shamshirband, S., "TiO_2 Nanotube Coating on Stainless Steel 304 for Biomedical Applications," *Ceremics Interntional.* Vol. 41, No. 2, pp. 2785-2793, 2015.

[21] Hurley, M.F., Olsen, C.R., Ward, L.J., Jaques, B.J., Johnson, K.A., Gunnerson, J.K., and Butt, D.P., "Transgranular Stress Corrosion Cracking of 304L Stainless Steel Pipe Clamps in Direct use Geothermal Water Heating Applications," *Engineering Failure Analysis.* Vol. 33, pp. 336-346, 2013.

[22] ASM International Handbook Committee., 1990. *Metals Handbook Vol. 1,* 10^{th} ed, Materials Park. Ohio.

[23] Di Martino, S.F., Faulkner, R.G., Hogg, S.C., Vujic, S., and Tassa, O., "Characterisation of Microstructure and Creep Properties of Alloy 617 for High-Temperature Applications," *Materials Science and Engineering: A,* Vol. 619, No. 1, pp. 77-86, 2014.

[24] Stewart, C.M., Gordon, A.P., Hogan, E.A., and Saxena, A., "Characterization of Creep Deformation and Rupture Behavior of DS GTD-111 Using the Kachanov-Rabotnov Constitutive Model," *Journal of Engineering Material Technology,* Vol. 133, No. 2, pp. 021013-1- 021013-2, 2011.

[25] Smith, H.H., Kullen, P.S., and Michel, D.J., "Fatigue Crack Propagation Behavior of Titanium Alloys 6242S and 5621S at Elevated Temperature," *Metallurgical and Materials Transactions A,* Vol. 19, No. 4, pp. 881-885, 1988.

[26] Davis, T.A., 2011. *MATLAB Primer*, CRC Press. Florida. pp. 157-180.